Journal of ELECTRICAL ENGINEERING, VOL 70 (2019), NO6, 429–442

sciendo

PAPERS

Banks of filters for implementation of DMWT of an image

Ondrej Kováč, Ján Mihalík*

We describee some possible options for implementation of the Discrete multiwavelet transform (DMWT) of an image by using filter banks. DMWT can be implemented by two channel bank of vector filters which are made by cross-connected scalar filters. The properties of DGHM, CL, BiHermite and SA4 multiwavelets are here analyzed, and compression analysis for output normalization of DMWT is performed. A procedure is design of equivalent replacing of 2 channel multifilters bank by 4 channel bank of single scalar filters. Finally, we deal with a possible reduction and combinations of subbands and suggest their use.

K e y w o r d s: multiwavelet, bank of filter, multifilter, DGHM, SA4, CL

1 Introduction

The discrete wavelet transform (DWT) and discrete multiwavelet transform (DMWT) became very popular in the last few decades. The transforms are used in a wide spectrum of applications, for example, we can mention compression [1-3], classification [4], multifocal and multi-exposure images fusion [5,6], medical image denoising [7], human emotion detection [8], image steganography [9,10] and many others. One of drawbacks of the classical DWT is that during the signal or image analysis it uses only one scale and one wavelet function. DMWT eliminates this drawback. DMWT works at least with 2 scale and 2 wavelet functions in contrast with the classical DWT [11,12]. The number of used functions is given by the parameter multiplicity r. The most common value of multiplicity for DMWT used in practice $r = 2$ and therefore we consider only this form of DMWT. The processor of DMWT can be realized by the bank of multifilters but this implementation is relatively difficult. We analyze a simplification of this DMWT implementation. DMWT implemented by multifilters bank which are preceded by prefilter. The matrix impulse responses of DMWT multifilters for 4 different multiwavelets is discussed and the connection of multifilters implemented by the cross-connected scalar filters are described. The method of cross-connected filter impulse responses creation from multifilters bank is described in detail and the transfer functions of filters for all considered multiwavelets are analyzed as well. Chapter 4 focuses on the analysis of output normality and compression properties of DMWT with considered multiwavelets. The cross-connected scalar filter implementation of the 2 channel multifilters bank (2CH) needs 4 scalar filters for each subband. Thus, 8 scalar filters are needed for LP (Lowpass) and HP (Highpass) band of MDWT. In addition the input signal has to be divided by pre-filtering [13] into 2 components which are brought to input of LP and HP filters [14]. Hence, we analyze the implementation of an equivalent 4 channel (4CH) bank of scalar single filters in chapter 5. The main benefit of this implementation is that on the outputs we get directly all 4 subbands of DMWT and in addition there is no need for the input image prefiltering. As a result, DMWT is realized only by 4 scalar single filters which means a significant simplification of its implementation. In the last chapter the possible methods of reduction and combination of DMWT subbands are analyzed. In this article some possible approaches and possibilities of subband combination for practical exploitation are described.

2 DMWT of image implemented by multifilters bank

Regardless of the used multiwavelets, a multiwavelet transform is implemented by banks of multifilters and multidecimators. The block diagram of one level multiwavelet transform with multiplicity $r = 2$ is in Fig. 1, showing one decomposition stage,having 2 inputs and 4 outputs. The multiplicity of outputs allows the input image analysis by multiple scaling and wavelet functions. Conventionally DMWT is performed as a convolution of the multifilter impulse response and the input vector signal. For DMWT wit $r = 2$ the low pass (LP) transfer function is given as a matrix $G_0(z) = \left[G^{(0)}_{l,m}(z)\right]_{2x2}$ $l, m \in \langle 1, 2\rangle$ and the high pass (HP) transfer function is described by matrix $G_1(z) = \left[G^{(1)}_{l,m}(z)\right]_{2x2}$ $l, m \in \langle 1, 2\rangle$.

The input are vector signals obtained by a prefiltering [1, 2] described by (1).

$$\begin{bmatrix} c_{0,1}(n) \\ c_{0,2}(n) \end{bmatrix} = \begin{bmatrix} f(2n) \\ f(2n+1) \end{bmatrix} \tag{1}$$

Faculty of Electrical Engineering and Informatics, Technical University of Košice, Letná 9, 042 00, Slovakia, ondrej.kovac@tuke.sk

DOI: 10.2478/jee-2019–0076, Print (till 2015) ISSN 1335-3632, On-line ISSN 1339-309X

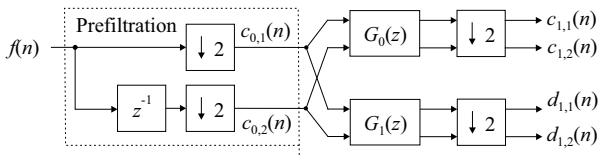

Fig. 1. Block diagram of one level DMWT

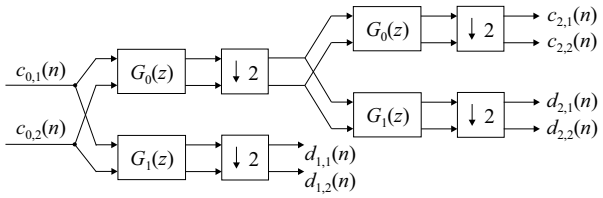

Fig. 3. Block diagram of two level DMWT

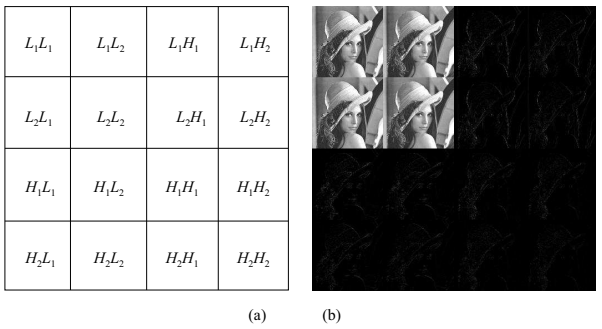

Fig. 2. General arrangement of subimages (a) – after one level DMWT, and (b) – the first level of image transformation

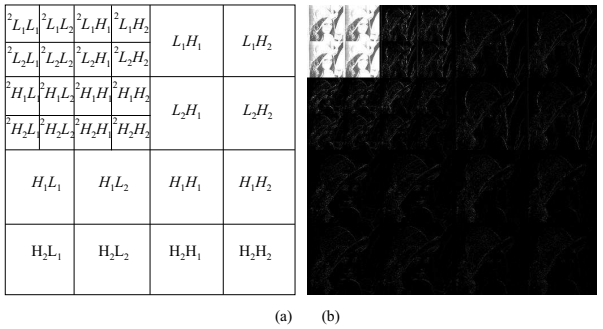

Fig. 4. General arrangement of subimages after (a) – the second level DMWT and (b) – the second level of lena image transformation

$$g_0(0) = \begin{bmatrix} \frac{3}{10} & \frac{2\sqrt{2}}{5} \\ -\frac{\sqrt{2}}{40} & -\frac{3}{20} \end{bmatrix} \quad g_0(1) = \begin{bmatrix} \frac{3}{10} & 0 \\ \frac{9\sqrt{2}}{40} & \frac{1}{2} \end{bmatrix} \quad g_0(2) = \begin{bmatrix} 0 & 0 \\ \frac{9\sqrt{2}}{40} & -\frac{3}{20} \end{bmatrix} \quad g_0(3) = \begin{bmatrix} 0 & 0 \\ -\frac{\sqrt{2}}{40} & 0 \end{bmatrix} \tag{2}$$

$$g_1(0) = \begin{bmatrix} -\frac{\sqrt{2}}{40} & -\frac{3}{20} \\ -\frac{1}{20} & -\frac{3\sqrt{2}}{20} \end{bmatrix} \quad g_1(1) = \begin{bmatrix} \frac{9\sqrt{2}}{40} & -\frac{1}{2} \\ \frac{9}{20} & 0 \end{bmatrix} \quad g_1(2) = \begin{bmatrix} \frac{9\sqrt{2}}{40} & -\frac{3}{20} \\ -\frac{9}{20} & \frac{3\sqrt{2}}{20} \end{bmatrix} \quad g_1(3) = \begin{bmatrix} -\frac{\sqrt{2}}{40} & 0 \\ \frac{1}{20} & 0 \end{bmatrix} \tag{3}$$

$$g_0(0) = \frac{1}{\sqrt{2}} \begin{bmatrix} \frac{1}{2} & \frac{-1}{2} \\ \frac{-1}{4} & \frac{1}{4} \end{bmatrix} \quad g_0(1) = \frac{1}{\sqrt{2}} \begin{bmatrix} 1 & 0 \\ 0 & \frac{\sqrt{7}}{2} \end{bmatrix} \quad g_0(2) = \frac{1}{\sqrt{2}} \begin{bmatrix} \frac{1}{2} & \frac{1}{2} \\ \frac{1}{4} & \frac{1}{4} \end{bmatrix} \tag{4}$$

$$g_1(0) = \frac{1}{\sqrt{2}} \begin{bmatrix} \frac{\sqrt{7}}{4} & -\frac{\sqrt{7}}{4} \\ \frac{1}{2} & -\frac{1}{2} \end{bmatrix} \quad g_1(1) = \frac{1}{\sqrt{2}} \begin{bmatrix} 0 & \frac{1}{2} \\ -1 & 0 \end{bmatrix} \quad g_1(2) = \frac{1}{\sqrt{2}} \begin{bmatrix} -\frac{\sqrt{7}}{4} & -\frac{\sqrt{7}}{4} \\ \frac{1}{2} & \frac{1}{2} \end{bmatrix} \tag{5}$$

$$g_0(0) = k \begin{bmatrix} 1 & \vartheta \\ \vartheta & 1 \end{bmatrix} \quad g_0(1) = k \begin{bmatrix} \vartheta^2 & \vartheta \\ \vartheta & \vartheta^2 \end{bmatrix} \quad g_0(2) = k \begin{bmatrix} \vartheta^2 & -\vartheta \\ -\vartheta & \vartheta^2 \end{bmatrix} \quad g_0(3) = k \begin{bmatrix} 1 & -\vartheta \\ -\vartheta & 1 \end{bmatrix} \tag{6}$$

$$g_1(0) = k \begin{bmatrix} 1 & -\vartheta \\ \vartheta & 1 \end{bmatrix} \quad g_1(1) = k \begin{bmatrix} -\vartheta^2 & \vartheta \\ -\vartheta & \vartheta^2 \end{bmatrix} \quad g_1(2) = k \begin{bmatrix} \vartheta^2 & \vartheta \\ -\vartheta & -\vartheta^2 \end{bmatrix} \quad g_1(3) = k \begin{bmatrix} -1 & -\vartheta \\ \vartheta & -1 \end{bmatrix} \tag{7}$$

If one stage of MDWT shown in Fig. 1 is connected into a cascade and the process of filtering is applied on the rows and subsequently on the columns of image the 2D DMWT is obtained [3]. At the output, the combined subimages are achieved. These subimages are arranged into the final representation of a DMWT image as Fig. 2(a) shows.

The same as in the classical DWT it is possible to continue in decomposition of LP subimages which leads to achievement of the second DMWT level. The block diagram of the 2 level DMWT is in Fig. 3. anbd it can be seen that the next levels are obtained directly from the outputs of previous levels. Thus, there is no prefiltering. The 2D DMWT of an image after the 2 level decomposition is shown in Fig. 4. After the second level of the transformation 28 subimages are obtained and they are arranged as shown in Fig. 4(a). For a better illustration in Fig. 4(b) DMWT of the Lena image after 2 levels of decomposition is shown.

3 Banks of multifilters

The concerned multiwavelets are DGHM [4], CL created by Chui and Lian [5], symmetric-antisymmetric SA4 [6,7] and BiHermite [8] therefore the article deals only with DMWT using these multiwavelets. Below equations (2),(3) define the impulse responses of two multifilters for DGHM.

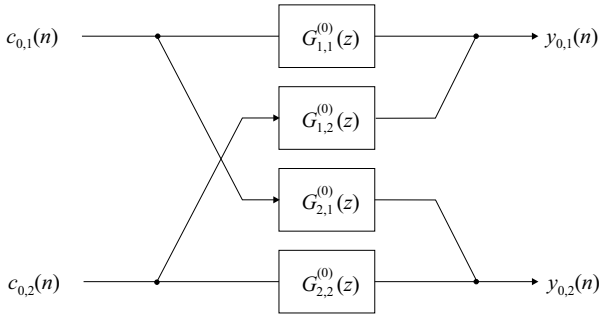

Fig. 5. Cross-connected scalar filters for realization of LP multifilter $G_0(z)$

For implementation of DMWT with multiwavelet CL the matrix impulse responses of multifilters are defined by (4),(5) and the impulse responses for SA4 multiwavelet by (6),(7), while the multiwavelet BiHermite is defined by (8),(9).

Multifilters $\boldsymbol{G}_0(z)$ and $\boldsymbol{G}_1(z)$ shown in Fig. 1 can be realized by the cross-connected scalar filters [14, 21]. Figure 5 shows such connection for an LP multifilter and an HP multifilter can be created in the same way.

The impulse responses of the individual scalar filters of DGHM LP multifilter are defined by (10)-(13) and HP filters are defined by (14-17).

The transfer functions of these scalar filters are shown in Fig. 6. It can be seen from plots in Fig. 6(a) that LP multifilter is created by scalar filters which have properties of both LP and HP filter. The transfer function of HP multifilter in Fig. 6(a) shows similar attributes. It can be seen from Fig. 6(a) that scalar filters with the impulse responses $g^0_{1,1}(n\ )$ a $g^0_{2,1}(n)$ are LP and the scalar filter $g^0_{2,2}(n)$ is HP. The scalar filter $g^0_{1,2}(n)$ is a band-

$$g_0(0) = \begin{bmatrix} \frac{\sqrt{2}}{4} & -\frac{\sqrt{2}}{4} \\ -\frac{1}{8\sqrt{2}} & \frac{1}{8\sqrt{2}} \end{bmatrix} \quad g_0(1) = \begin{bmatrix} \frac{\sqrt{2}}{2} & 0 \\ 0 & \frac{1}{2\sqrt{2}} \end{bmatrix} \quad g_0(2) = \begin{bmatrix} \frac{\sqrt{2}}{4} & \frac{\sqrt{2}}{8} \\ \frac{1}{8\sqrt{2}} & \frac{1}{8\sqrt{2}} \end{bmatrix} \tag{8}$$

$$g_1(0) = \begin{bmatrix} \frac{3\sqrt{2}}{16} & -\frac{\sqrt{2}}{16} \\ -\frac{1}{4\sqrt{2}} & \frac{3}{8\sqrt{2}} \end{bmatrix} \quad g_1(1) = \begin{bmatrix} 0 & \frac{\sqrt{2}}{4} \\ \frac{1}{2\sqrt{2}} & 0 \end{bmatrix} \quad g_1(2) = \begin{bmatrix} -\frac{3\sqrt{2}}{16} & -\frac{\sqrt{2}}{16} \\ -\frac{1}{4\sqrt{2}} & -\frac{3}{8\sqrt{2}} \end{bmatrix} \tag{9}$$

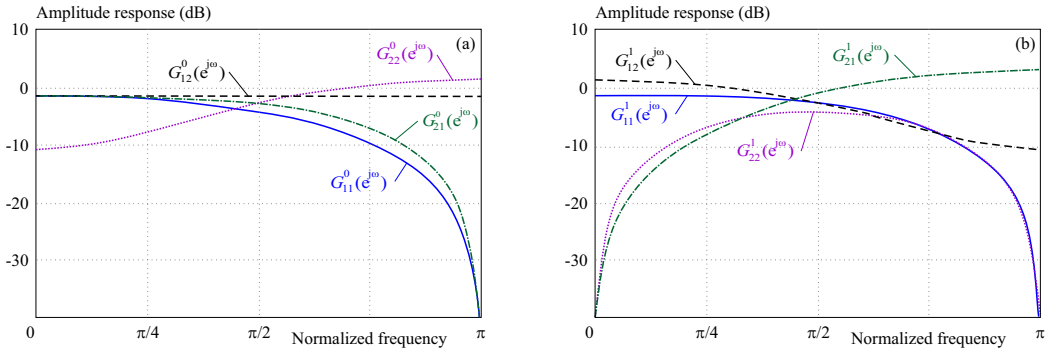

Fig. 6. Transfer functions of individual scalar filters of cross-connected (a)– LP, and (b) – HP multifilter for DGHM multiwavelet

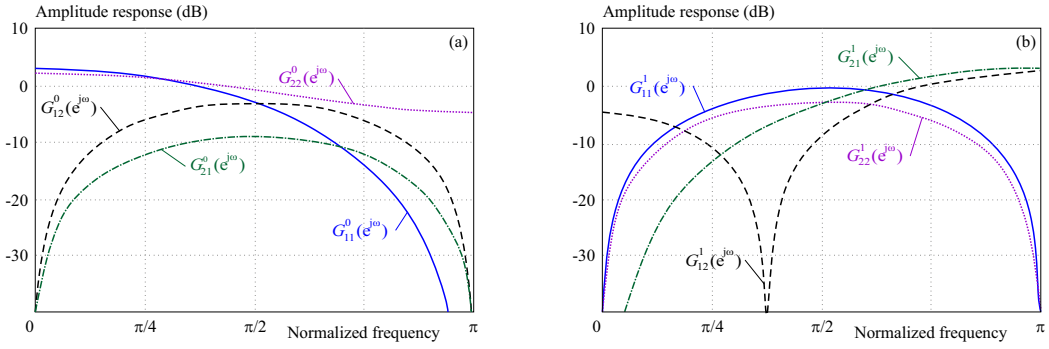

Fig. 7. Transfer functions of individual scalar filters of cross-connected (a) – LP, and (b) – HP multifilter for CL multiwavelet

pass (BP) filter with constant attenuation in the whole frequency band.

Plots in Fig. 6(a) show that the scalar filters $g^1_{1,1}(n)$ and $g^1_{1,2}(n)$ are LP, the filter $g^1_{2,2}(n)$ is HP and $g^1_{2,2}(n)$ is BP. The transfer functions of scalar filters in Fig. 6 are crossed circa in the middle point $\omega = \pi/2$ of a frequency band. The impulse responses for another multiwavelets are obtained in the same way. The impulse response for multiwavelet CL are defined by (18-25) and the transfer functions of these filters are shown in Fig. 7.

In contrast with the multifilters for implementation of DGHM the character of scalar filters for CL corresponds to the character of a particular multifilter. LP multifilter with transfers in Fig. 7(a) is created by the LP scalar filters $g^0_{1,1}(n), g^0_{2,2}(n)$ and the BP scalar filters $g^0_{1,2}(n), g^0_{2,1}(n)$. The HP multifilter, Fig. 7(b), is created by the HP scalar filters $g^1_{1,2}(n), g^1_{2,1}(n)$ and the BP scalar filters $g^1_{1,1}(n), g^1_{2,2}(n)$.

Impulse responses for BiHermite multiwavelet are defined by the next equations (26-33) and its transfer functions are shown in Fig. 8.

LP multifilter is created by scalar filters with LP and BP character as it can be seen from Fig. 8(a). For this multifilter LP scalar filter is dominant with the im-

$$G^{(0)}_{1,1}(z) \to g^0_{1,1}(n) = \left\{\frac{3}{10}, \frac{3}{10}\right\} \quad (10)$$

$$G^{(0)}_{1,2}(z) \to g^0_{1,2}(n) = \left\{\frac{2\sqrt{2}}{5}\right\} \quad (11)$$

$$G^{(0)}_{2,1}(z) \to g^0_{2,1}(n) = \left\{-\frac{\sqrt{2}}{40}, \frac{9\sqrt{2}}{40}, \frac{9\sqrt{2}}{40}, -\frac{\sqrt{2}}{40}\right\} \quad (12)$$

$$G^{(0)}_{2,2}(z) \to g^0_{2,2}(n) = \left\{-\frac{3}{20}, \frac{1}{2}, -\frac{3}{20}\right\} \quad (13)$$

$$G^{(1)}_{1,1}(z) \to g^1_{1,1}(n) = \left\{-\frac{\sqrt{2}}{40}, \frac{9\sqrt{2}}{40}, \frac{9\sqrt{2}}{40}, -\frac{\sqrt{2}}{40}\right\} \quad (14)$$

$$G^{(1)}_{1,2}(z) \to g^1_{1,2}(n) = \left\{-\frac{3}{20}, -\frac{1}{2}, -\frac{3}{20}\right\} \quad (15)$$

$$G^{(1)}_{2,1}(z) \to g^1_{2,1}(n) = \left\{-\frac{1}{20}, \frac{9}{20}, -\frac{9}{20}, \frac{1}{20}\right\} \quad (16)$$

$$G^{(1)}_{2,2}(z) \to g^1_{2,2}(n) = \left\{-\frac{3\sqrt{2}}{20}, 0, \frac{3\sqrt{2}}{20}\right\} \quad (17)$$

$$g^0_{1,1}(n) = \left\{\frac{1}{2\sqrt{2}}, \frac{1}{\sqrt{2}}, \frac{1}{2\sqrt{2}}\right\} \quad (18)$$

$$g^0_{1,2}(n) = \left\{-\frac{1}{2\sqrt{2}}, 0, \frac{1}{2\sqrt{2}}\right\} \quad (19)$$

$$g^0_{2,1}(n) = \left\{-\frac{1}{4\sqrt{2}}, 0, \frac{1}{4\sqrt{2}}\right\} \quad (20)$$

$$g^0_{2,2}(n) = \left\{\frac{1}{4\sqrt{2}}, \frac{\sqrt{7}}{2\sqrt{2}}, \frac{1}{4\sqrt{2}}\right\} \quad (21)$$

$$g^1_{1,1}(n) = \left\{\frac{\sqrt{7}}{4\sqrt{2}}, 0, -\frac{\sqrt{7}}{4\sqrt{2}}\right\} \quad (22)$$

$$g^1_{1,2}(n) = \left\{-\frac{\sqrt{7}}{4\sqrt{2}}, \frac{1}{2\sqrt{2}}, -\frac{\sqrt{7}}{4\sqrt{2}}\right\} \quad (23)$$

$$g^1_{2,1}(n) = \left\{\frac{1}{2\sqrt{2}}, -\frac{1}{\sqrt{2}}, \frac{1}{2\sqrt{2}}\right\} \quad (24)$$

$$g^1_{2,2}(n) = \left\{-\frac{1}{2\sqrt{2}}, 0, \frac{1}{2\sqrt{2}}\right\} \quad (25)$$

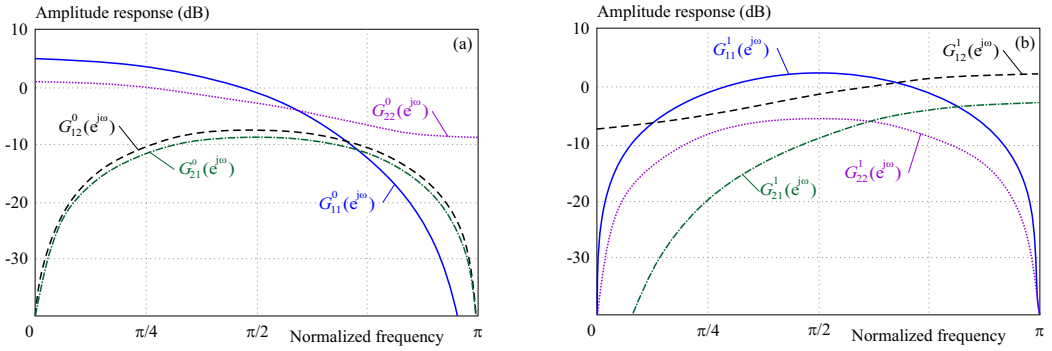

Fig. 8. Transfer functions of individual scalar filters of cross-connected (a) – LP, and (b) – HP multifilter for BiHermite multiwavelet

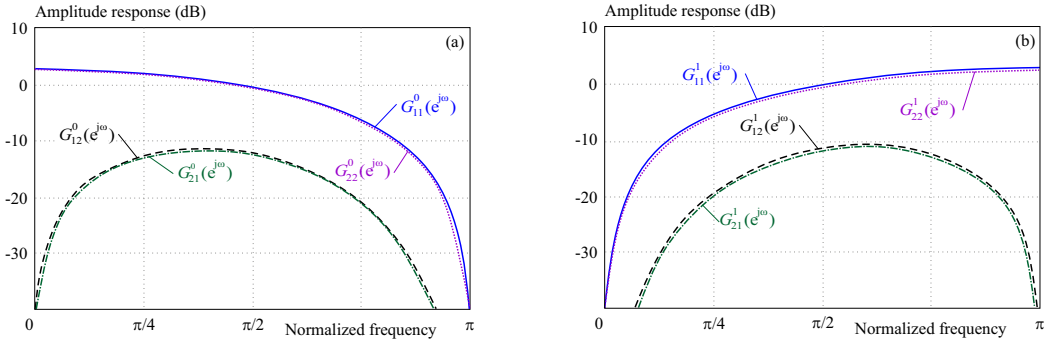

Fig. 9. Transfer functions of individual scalar filters of cross-connected (a) – LP, and (b) – HP multifilter for SA4 multiwavelet

$$g^0_{1,1}(n) = \left\{\frac{\sqrt{2}}{4}, \frac{\sqrt{2}}{2}, \frac{\sqrt{2}}{4}\right\} \quad (26)$$

$$g^0_{1,2}(n) = \left\{-\frac{\sqrt{2}}{4}, 0, \frac{\sqrt{2}}{8}\right\} \quad (27)$$

$$g^0_{2,1}(n) = \left\{-\frac{1}{8\sqrt{2}}, 0, \frac{1}{8\sqrt{2}}\right\} \quad (28)$$

$$g^0_{2,2}(n) = \left\{\frac{1}{8\sqrt{2}}, \frac{1}{2\sqrt{2}}, \frac{1}{8\sqrt{2}}\right\} \quad (29)$$

$$g^1_{1,1}(n) = \left\{\frac{3\sqrt{2}}{16}, 0, -\frac{3\sqrt{2}}{16}\right\} \quad (30)$$

$$g^1_{1,2}(n) = \left\{-\frac{\sqrt{2}}{16}, \frac{\sqrt{2}}{4}, -\frac{\sqrt{2}}{16}\right\} \quad (31)$$

$$g^1_{2,1}(n) = \left\{-\frac{1}{4\sqrt{2}}, \frac{1}{2\sqrt{2}}, -\frac{1}{4\sqrt{2}}\right\} \quad (32)$$

$$g^1_{2,1}(n) = \left\{\frac{3}{8\sqrt{2}}, 0, -\frac{3}{8\sqrt{2}}\right\} \quad (33)$$

$$g^0_{1,1}(n) = \left\{k, k\vartheta^2, k\vartheta^2, k\right\} \quad (34)$$

$$g^0_{1,2}(n) = \{k\vartheta, k\vartheta, -k\vartheta, -k\vartheta\} \quad (35)$$

$$g^0_{2,1}(n) = \{k\vartheta, k\vartheta, -k\vartheta, -k\vartheta\} \quad (36)$$

$$g^0_{2,2}(n) = \left\{k, k\vartheta^2, k\vartheta^2, k\right\} \quad (37)$$

$$g^1_{1,1}(n) = \left\{k, -k\vartheta^2, k\vartheta^2, -k\right\} \quad (38)$$

$$g^1_{1,2}(n) = \{-k\vartheta,\ k\vartheta,\ k\vartheta,\ -k\vartheta\} \quad (39)$$

$$g^1_{2,1}(n) = \{k\vartheta, -k\vartheta, -k\vartheta,\ k\vartheta\} \quad (40)$$

$$g^1_{2,2}(n) = \left\{k, k\vartheta^2, -k\vartheta^2, k\right\} \quad (41)$$

where, $\vartheta = 4 + \sqrt{15}$ and $k = \dfrac{1}{(\vartheta^2+1)\sqrt{2}}$

pulse response $g^0_{1,1}(n)$ which represents amplification for $\omega \in (0; \pi/2)$. The scalar filter with the impulse response $g^0_{2,2}(n)$ roughly allows frequencies until $\omega = \pi/2$. Fig. 8(b) shows transfer functions for HP multifilter. For HP multifilter it can be concluded that scalar filters are of BP and HP character. Amplification is provided by scalar filters with the impulse responses $g^1_{1,1}(n)$ and $g^1_{1,2}(n)$ for frequencies $\omega \in (\pi/4; 2\pi)$. The multifilters for implementation of DMWT with SA4 multiwavelet are defined by (34 -41).

The transfer functions of scalar filters for a bank with SA4 multiwavelet are shown in Fig. 9. Contrary to the other mentioned multiwavelet banks the transfer functions of LP and HP scalar filters for SA4 show a considerable symmetry and some of them are the same. In general it is possible to conclude that LP and HP scalar filters have the same character as LP and HP multifilter which they implement.

4 Analysis of compression properties of DMWT

The compression properties of individual multi-wavelets are evaluated in this part of the article. The evaluation is done on the base of the ratio of energy stored in subimages and energy of an input image. This comparison can be done only if the output of DMWT is normalized. Thus, the energy of the image after the transform E_{DMWT} and the energy before the transform E_{IMG} have to be equal.

$$\frac{E_{\mathrm{DMWT}}}{E_{\mathrm{IMG}}} \quad (42)$$

This ratio for each multi-wavelet was verified on 72 test images [22] which were transformed and subsequently the energy ratios were computed. The results are listed in Tab. 1.

Table 1. Statistical evaluation of energy ratio between original and transformed image for DGHM, CL, BiHermite and SA4 multiwavelet

Multi wavelet	Mean of ratio $E_{\mathrm{DMWT}}/E_{\mathrm{IMG}}$	Standard deviation
DGHM	0.2503	0.0011
CL	0.9992	0.0098
BiHermite	0.1714	0.0020
SA4	1.0003	0.0039

It is clear from Tab. 1 that output of DMWT with CL and SA4 multiwavelet are normalized but it is necessary to adjust multifilters for DGHM and BiHermite multiwavelets. For DGHM it is sufficient to multiply each multifilter with a constant o $\sqrt{2}$ f. Equations (43 and 44) define the normalized impulse responses. By the same process it was concluded that the first row of multifilters for multiwavelet BiHermite has to be multiplied by a constant of $\sqrt{\frac{27}{5}}$. The corrected BiHermite multifilter impulse responses are defined by equations (45 and 46).

The mean values of the defined energy ratio (42) for DGHM and BiHermite multiwavelets are listed in Tab. 2.

Table 2. Statistical evaluation of energy ratio between original and transformed image for normalized multiwavelet DGHM and BiHermite

Multi wavelet	Mean of ratio $E_{\mathrm{DMWT}}/E_{\mathrm{IMG}}$	Standard deviation
DGHM	1.0000	0.0008
BiHermite	1.0055	0.0177

DMWT with each multiwavelet for the Lena image with the subband energy distribution is shown in Fig. 10. The transformed images are shown in their absolute value for a better illustration.

On the base of the energy distribution shown in Fig. 10 it can be concluded that the energy of image is concentrated in the LP band (L_1L_1, L_1L_2, L_2L_1 and L_2L_2 subimages). The transform with the DGHM multiwavelet

$$g_0(0) = \sqrt{2}\begin{bmatrix} \frac{3}{10} & \frac{2\sqrt{2}}{5} \\ -\frac{\sqrt{2}}{40} & -\frac{3}{20} \end{bmatrix} \quad g_0(1(= \sqrt{2}\begin{bmatrix} \frac{3}{10} & 0 \\ \frac{9\sqrt{2}}{40} & \frac{1}{2} \end{bmatrix} \quad g_0(2(= \sqrt{2}\begin{bmatrix} 0 & 0 \\ \frac{9\sqrt{2}}{40} & -\frac{3}{20} \end{bmatrix} \quad g_0(3(= \sqrt{2}\begin{bmatrix} 0 & 0 \\ -\frac{\sqrt{2}}{40} & 0 \end{bmatrix} \tag{43}$$

$$g_1(0(= \sqrt{2}\begin{bmatrix} -\frac{\sqrt{2}}{40} & -\frac{3}{20} \\ -\frac{1}{20} & -\frac{3\sqrt{2}}{20} \end{bmatrix} \quad g_1(1(= \sqrt{2}\begin{bmatrix} \frac{9\sqrt{2}}{40} & -\frac{1}{2} \\ \frac{9}{20} & 0 \end{bmatrix} \quad g_1(2(= \sqrt{2}\begin{bmatrix} \frac{9\sqrt{2}}{40} & -\frac{3}{20} \\ -\frac{9}{20} & \frac{3\sqrt{2}}{20} \end{bmatrix} \quad g_1(3(= \sqrt{2}\begin{bmatrix} -\frac{\sqrt{2}}{40} & 0 \\ \frac{1}{20} & 0 \end{bmatrix} \tag{44}$$

$$g_0\,(0) = \begin{bmatrix} \sqrt{\frac{27}{5}}\frac{\sqrt{2}}{4} & -\sqrt{\frac{27}{5}}\frac{\sqrt{2}}{4} \\ -\frac{1}{8\sqrt{2}} & \frac{1}{8\sqrt{2}} \end{bmatrix} \quad g_0\,(1) = \begin{bmatrix} \sqrt{\frac{27}{5}}\frac{\sqrt{2}}{2} & 0 \\ 0 & \frac{1}{2\sqrt{2}} \end{bmatrix} \quad g_0\,(2) = \begin{bmatrix} \sqrt{\frac{27}{5}}\frac{\sqrt{2}}{4} & \sqrt{\frac{27}{5}}\frac{\sqrt{2}}{8} \\ \frac{1}{8\sqrt{2}} & \frac{1}{8\sqrt{2}} \end{bmatrix} \tag{45}$$

$$g_1\,(0) = \begin{bmatrix} \sqrt{\frac{27}{5}}\frac{3\sqrt{2}}{16} & -\sqrt{\frac{28}{5}}\frac{\sqrt{2}}{16} \\ -\frac{1}{4\sqrt{2}} & \frac{3}{8\sqrt{2}} \end{bmatrix} \quad g_1\,(1) = \begin{bmatrix} 0 & \sqrt{\frac{27}{5}}\frac{\sqrt{2}}{4} \\ \frac{1}{2\sqrt{2}} & 0 \end{bmatrix} \quad g_1\,(2) = \begin{bmatrix} -\sqrt{\frac{27}{5}}\frac{3\sqrt{2}}{16} & -\sqrt{\frac{27}{5}}\frac{\sqrt{2}}{16} \\ -\frac{1}{4\sqrt{2}} & -\frac{3}{8\sqrt{2}} \end{bmatrix} \tag{46}$$

45.59	19.82	1.99	0.11
19.78	8.61	0.88	0.08
1.93	0.86	0.11	0.04
0.07	0.06	0.03	0.05

24.95	20.58	4.32	0.09
20.62	17.01	3.55	0.06
4.29	3.53	0.79	0.05
0.06	0.04	0.04	0.02

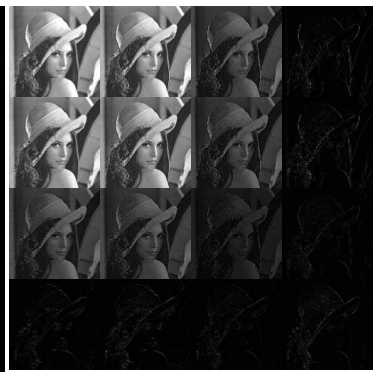

(a) (b)

(c) (d)

45.09	18.73	3.27	0.05
18.74	7.78	1.34	0.02
3.10	1.27	0.51	0.03
0.03	0.01	0.03	0.00

24.70	24.78	0.09	0.13
24.73	24.82	0.10	0.15
0.05	0.06	0.03	0.05
0.08	0.01	0.05	0.07

Fig. 10. Image transformed by DMWT and its subimage energy distribution in % for normalized multiwavelet (a) – DGHM, (b) – CL, (c) – BiHermite, and (d) – SA4

concentrates 93.8% of the energy in the LP subimages, for CL it is 83.16%, for BiHermite 90.34% and the highest compression of 99.03% is achieved by SA4 multiwavelet. It can be seen that SA4 in the other subimages concentrates less than 1% of the total energy. Other multiwavelets left much more energy in HP subimages. The

Table 3. Mean energy values of LP band for DMWT with DGHM, CL, BiHermite and SA4 multiwavelet

Multiwavelet	L-subband	Mean(%)	Std(%)
DGHM	L_1L_1	44.7085	2.0528
	L_1L_2	19.4907	0.6716
	L_2L_1	19.5289	0.6652
	L_2L_2	8.5517	0.1689
	L_{sum}	92.2772	3.4387
CL	L_1L_1	24.5937	0.9901
	L_1L_2	20.2894	0.7375
	L_2L_1	20.2659	0.7570
	L_2L_2	16.7556	0.8067
	L_{sum}	81.9048	2.9194
BiHermite	L_1L_1	43.9182	2.4780
	L1L2	18.2835	1.0079
	L_2L_1	18.2765	1.0120
	L_2L_2	7.6170	0.4976
	L_{sum}	88.0946	4.7957
SA4	L_1L_1	24.1023	1.3032
	L_1L_2	24.3110	1.0408
	L_2L_1	24.3228	0.9990
	L_2L_2	24.5620	0.9140
	L_{sum}	97.2976	4.0311

comparison of the mean value energy stored in LP subbands is shown in Tab. 3.

These values were obtained on the base of transform of 72 different images.

Table 3 shows that DMWT with SA4 multiwavelet achieved the highest energy compression into LP subimages. In accordance with the previous experiments shown in Fig. 10 it can be concluded that the energy for SA4 is distributed evenly into the L subband, contrary to this other multiwavelets concentrate the energy into L_1L_1 subimage. On the base of standard deviation values it can be concluded that DMWT with BiHermite multiwavelet is the most sensitive to the image content and on the other hand CL multiwavelet is less sensitive to image content changes.

5 Banks of single filters

Banks of multifilters used for implementation of DMWT are created by the cross-connected scalar filters. These 2 channel (2CH) banks implement LP (approximation) and HP (detail) subbands. The realization of DMWT in this way is not very advantageous. It needs 8 scalar filters which are in addition preceded by multifilters. These prefilters perform change of the input signal from scalar form to its vector form. An equivalent replacement of 2CH multifilters bank by four channel (4CH) single filter bank [23] shown in Fig. 11 was analyzed.

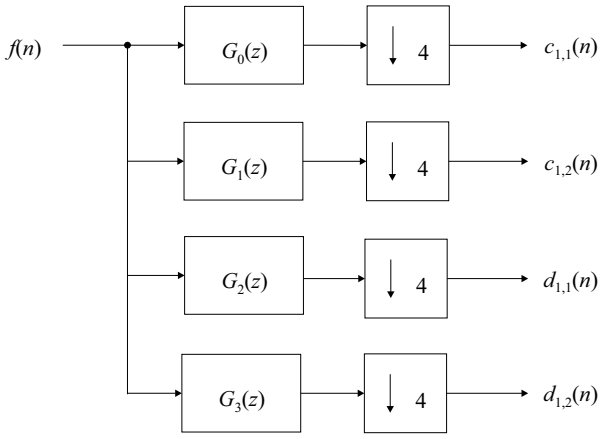

Fig. 11. Equivalent 4ch single filter bank

Figure 11 shows that 4CH single filter bank implementation of DMWT does not need prefiltering as it was seen in the case of 2CH multifilters bank. The input signal is brought directly on the input of this equivalent 4CH bank. This signal is subsequently filtered by scalar filters in 4 parallel branches. After decimation by factor 4 all subbands of DMWT are directly obtained on the outputs of these branches. Scalar filters with the transfer functions $G_0(z)$ and $G_1(z)$ implement LP subimages and on the other hand filters with the transfer functions $G_2(z)$ and $G_3(z)$ implement HP subbands. The transfer functions are created from scalar filters of 2CH multifilter bank by using (47-50).

In (49 and 50) a substitution of $z \to z^2$ is used. This substitution is caused by the order change of filtering and decimation [24]. The mathematical process of replacement of 2CH multifilter bank by 4CH single filters bank for DGHM multiwavelet is shown in the next text.

$$\underline{\boldsymbol{G}}_0(z) = \begin{bmatrix} G^0_{1,1}(z) & G^0_{1,2}(z) \\ G^0_{2,1}(z) & G^0_{2,2}(z) \end{bmatrix} \quad (47)$$

$$\underline{\boldsymbol{G}}_1(z) = \begin{bmatrix} G^1_{1,1}(z) & G^1_{1,2}(z) \\ G^1_{2,1}(z) & G^1_{2,2}(z) \end{bmatrix} \quad (48)$$

$$\begin{bmatrix} G_0(z) \\ G_1(z) \end{bmatrix} = \underline{\boldsymbol{G}}^0(z^2) \begin{bmatrix} 1 \\ z \end{bmatrix} \quad (49)$$

$$\begin{bmatrix} G_2(z) \\ G_3(z) \end{bmatrix} = \underline{\boldsymbol{G}}^1(z^2) \begin{bmatrix} 1 \\ z \end{bmatrix} \quad (50)$$

In (49 and 50) a substitution of $z \to z^2$ is used. This substitution is caused by the order change of filtering and decimation [24]. The mathematical process of replacement of 2CH multifilter bank by 4CH single filters bank for DGHM multiwavelet is shown in the next text.

$$\underline{\boldsymbol{G}}_0(z) = \sqrt{2}\begin{bmatrix} \frac{3}{10}z^0 + \frac{3}{10}z^{-1} & \frac{2\sqrt{2}}{5}z^0 \\ -\frac{\sqrt{2}}{40}z^0 + \frac{9\sqrt{2}}{40}z^{-1} + \frac{9\sqrt{2}}{40}z^{-2} - \frac{\sqrt{2}}{40}z^{-3}; & -\frac{3}{20}z^0 + \frac{1}{2}z^{-1} - \frac{3}{20}z^{-2} \end{bmatrix} \tag{51}$$

$$\underline{\boldsymbol{G}}_0\left(z^2\right) = \sqrt{2}\begin{bmatrix} \frac{3}{10}z^0 + \frac{3}{10}z^{-2}; & \frac{2\sqrt{2}}{5}z^0 \\ -\frac{\sqrt{2}}{40}z^0 + \frac{9\sqrt{2}}{40}z^{-2} + \frac{9\sqrt{2}}{40}z^{-4} - \frac{\sqrt{2}}{40}z^{-6}; & -\frac{3}{20}z^0 + \frac{1}{2}z^{-1} - \frac{3}{20}z^{-4} \end{bmatrix} \tag{52}$$

$$\begin{bmatrix} G_(z) \\ G_1(z) \end{bmatrix} = \underline{\boldsymbol{G}}_0(z^2)\begin{bmatrix} 1 \\ z \end{bmatrix} = \sqrt{2}\begin{bmatrix} \frac{2\sqrt{2}}{5}z + \frac{3}{10} + \frac{3}{10}z^{-2} \\ -\frac{3}{20}z - \frac{\sqrt{2}}{40} + \frac{1}{2}z^{-1} + \frac{9\sqrt{2}}{40}z^{-2} - \frac{3}{20}z^{-3} + \frac{9\sqrt{2}}{40}z^{-4} - \frac{\sqrt{2}}{40}z^{-6} \end{bmatrix} \tag{53}$$

The impulse responses for these transfer functions are

$$\begin{bmatrix} g_0(n) \\ g_1(n) \end{bmatrix} = \sqrt{2}\begin{bmatrix} \frac{2\sqrt{2}}{5} & \frac{3}{10} & 0 & \frac{3}{10} & 0 & 0 & 0 & 0 \\ -\frac{3}{20} & -\frac{\sqrt{2}}{40} & \frac{1}{2} & \frac{9\sqrt{2}}{40} & -\frac{3}{20} & \frac{9\sqrt{2}}{40} & 0 & -\frac{\sqrt{2}}{40} \end{bmatrix} \tag{54}$$

The impulse responses in (54) implement LP filters. For HP transfer functions we can write (55). Thus, the impulse responses for HP subband are defined by (56).

$$\begin{bmatrix} G_2(z) \\ G_3(z) \end{bmatrix} = \sqrt{2}\begin{bmatrix} -\frac{3}{20}z - \frac{\sqrt{2}}{40} - \frac{1}{2}z^{-1} + \frac{9\sqrt{2}}{40}z^{-2} - \frac{3}{20}z^{-3} + \frac{9\sqrt{2}}{40}z^{-4} - \frac{\sqrt{2}}{40}z^{-6} \\ -\frac{3\sqrt{2}}{20}z - \frac{1}{20} + \frac{9}{20}z^{-2} + \frac{3\sqrt{2}}{20}z^{-3} - \frac{9}{20}z^{-4} + \frac{1}{20}z^{-6} \end{bmatrix} \tag{55}$$

$$\begin{bmatrix} g_2(n) \\ g_3(n) \end{bmatrix} = \sqrt{2}\begin{bmatrix} -\frac{3}{20} & -\frac{\sqrt{2}}{40} & -\frac{1}{2} & \frac{9\sqrt{2}}{40} & -\frac{3}{20} & \frac{9\sqrt{2}}{40} & 0 & -\frac{\sqrt{2}}{40} \\ -\frac{3\sqrt{2}}{20} & -\frac{1}{20} & 0 & \frac{9}{20} & \frac{3\sqrt{2}}{20} & -\frac{9}{20} & 0 & \frac{1}{20} \end{bmatrix} \tag{56}$$

The impulse responses in (54) implement LP filters. For HP transfer functions we can write (55). Thus, the impulse responses for HP subband are defined by (56).

For impulse responses in (54) and (56) we can display the transfer functions shown in Fig. 12(a) and therefore it can be concluded that each of these scalar filters show amplification in a different part of the frequency spectrum. The filter with the transfer $G_0(z)$ covers the first quarter of the frequency band. In the second and third part the frequency band is covered by the transfer $G_3(z)$ and $G_1(z)$. The last part of the band is covered by filter with the transfer $G_2(z)$. Filters behave as attenuation in the other parts of the frequency band. The filters $G_0(z)$ and $G_1(z)$ implement a scale function, which presents an approximation of the input signal. It is clear from Fig. 12(a), that these filters attenuate the input signal for frequencies $\omega \in (\pi/4, \pi/2)(3\pi/4, \pi)$ and on the other hand the filters $G_2(z)$ a $G_3(z)$ implement wavelet functions which represent details of the input image. These filters attenuate the input signal for $\omega \in (0, \pi/4)$ as it can be seen from Fig. 12(a).

The impulse responses and transfer functions for other multiwavelets can be obtained in the same way as for DGHM multiwavelet. To be completely, the impulse responses for CL, BiHermite and SA4 multiwavelets are mentioned in the next part of the article.

The impulse responses of 4CH bank of single filter for DMWT with CL multiwavelets are defined by (57-60) and transfer functions are in Fig. 12(b). These functions show similar properties as it was observed for DGHM multiwavelet. Each filter shows amplification for different quarter of the frequency band. Thus, each frequency band of the transformed signal is created by frequencies of the particular quarter and only in small contribution by frequencies of the other bands. The LP filters $G_0(z)$ and $G_1(z)$ present more likely a band stop for frequencies $\omega \in (\pi/4, 3\pi/4)$ and on the other hand, the HP filters $G_2(z)$ and $G_3(z)$ present a band pass in this subband. The filter $G_2(z)$ allows frequencies for $\omega \in (\pi/4, \pi/2)$ and

$$g_0(n) = \frac{1}{\sqrt{2}}\left[-\frac{1}{2} \quad \frac{1}{2} \quad 0 \quad 1 \quad \frac{1}{2} \quad \frac{1}{2}\right] \tag{57}$$

$$g_1(n) = \frac{1}{\sqrt{2}}\left[\frac{1}{4} \quad -\frac{1}{4} \quad \frac{\sqrt{7}}{2} \quad 0 \quad \frac{1}{4} \quad \frac{1}{4}\right] \tag{58}$$

$$g_2(n) = \frac{1}{\sqrt{2}}\left[-\frac{\sqrt{7}}{4} \quad \frac{\sqrt{7}}{4} \quad \frac{1}{2} \quad 0 \quad -\frac{\sqrt{7}}{4} \quad -\frac{\sqrt{7}}{4}\right] \tag{59}$$

$$g_3(n) = \frac{1}{\sqrt{2}}\left[-\frac{1}{2} \quad \frac{1}{2} \quad 0 \quad -1 \quad \frac{1}{2} \quad \frac{1}{2}\right] \tag{60}$$

$$g_0(n) = \sqrt{\frac{28}{5}}\left[\frac{\sqrt{2}}{4} \quad \frac{\sqrt{2}}{4} \quad 0 \quad \frac{\sqrt{2}}{2} \quad -\frac{\sqrt{2}}{8} \quad \frac{\sqrt{2}}{4}\right] \tag{61}$$

$$g_1(n) = \left[\frac{1}{8\sqrt{2}} \quad -\frac{1}{8\sqrt{2}} \quad \frac{1}{2\sqrt{2}} \quad 0 \quad \frac{1}{8\sqrt{2}} \quad \frac{1}{8\sqrt{2}}\right] \tag{62}$$

$$g_2(n) = \sqrt{\frac{28}{5}}\left[-\frac{\sqrt{2}}{16} \quad \frac{3\sqrt{2}}{16} \quad \frac{\sqrt{2}}{4} \quad 0 \quad \frac{\sqrt{2}}{16} \quad -\frac{3\sqrt{2}}{16}\right] \tag{63}$$

$$g_3(n) = \left[\frac{3}{8\sqrt{2}} \quad -\frac{1}{4\sqrt{2}} \quad 0 \quad \frac{1}{2\sqrt{2}} \quad -\frac{3}{8\sqrt{2}} \quad -\frac{1}{4\sqrt{2}}\right] \tag{64}$$

$$g_0(n) = k\,[\vartheta \quad 1 \quad \vartheta \quad \vartheta^2 \quad -\vartheta \quad \vartheta^2 \quad -\vartheta \quad 1] \tag{65}$$

$$g_1(n) = k\,[1 \quad \vartheta \quad \vartheta^2 \quad \vartheta \quad \vartheta^2 \quad -\vartheta \quad 1 \quad -\vartheta] \tag{66}$$

$$g_2\,(n) = k\,[-\vartheta \quad 1 \quad \vartheta \quad -\vartheta^2 \quad \vartheta \quad \vartheta^2 \quad -\vartheta \quad -1] \tag{67}$$

$$g_3\,(n) = k\,[1 \quad \vartheta \quad \vartheta^2 \quad -\vartheta \quad -\vartheta^2 \quad -\vartheta \quad -1 \quad \vartheta] \tag{68}$$

where $\vartheta = 4 + \sqrt{15}$ a $k = \frac{1}{\sqrt{2}}\frac{1}{\vartheta^2+1}$

the filter $G_3(z)$ allows frequencies for $\omega \in (\pi/2, 3\pi/4)$. The impulse response of 4CH bank of single filters for DMWT with BiHermite multiwavelet are given by (61-64) and the transfer functions are in Fig. 12(c).

For impulse responses in (54 and 56) we can display the transfer functions shown in Fig. 12(a) and therefore it can be concluded that each of these scalar filters show amplification in a different part of the frequency spectrum. The filter with the transfer $G_0(z)$ covers the first quarter of the frequency band. In the second and third part the frequency band is covered by the transfer $G_3(z)$ and $G_1(z)$. The last part of the band is covered by filter with the transfer $G_2(z)$. Filters behave as attenuation in the other parts of the frequency band. The filters $G_0(z)$ and $G_1(z)$ implement a scale function, which presents an approximation of the input signal. It is clear from Fig. 12(a), that these filters attenuate the input signal for frequencies $\omega \in \left(\frac{\pi}{4}\,,\ \frac{\pi}{2}\right) \cup \left(\frac{3\pi}{4}\,,\ \pi\right)$ and on the other hand the filters $G_2(z)$ a $G_3(z)$ implement wavelet functions which represent details of the input image. These filters attenuate the input signal for $\omega \in \left(0,\ \frac{\pi}{4}\right)$ as it can be seen from Fig. 12(a).

The impulse responses and transfer functions for other multiwavelets can be obtained in the same way as for DGHM multiwavelet. To be completely, the impulse responses for CL, BiHermite and SA4 multiwavelets are mentioned in the next part of the article. The impulse responses of 4CH bank of single filter for DMWT with CL multiwavelets are defined by (57-60)

The filters described by impulse responses (57-60) have transfer functions depicted in Fig. 12(b). These functions show similar properties as it was observed for DGHM multiwavelet. Each filter shows amplification for different quarter of the frequency band. Thus, each frequency band of the transformed signal is created by frequencies of the quarter and only in small contribution by frequencies of the other bands. The LP filters $G_0(z)$ and $G_1(z)$ present more likely a band stop for frequencies $\omega \in \left(\frac{\pi}{4}\,,\ \frac{3\pi}{4}\right)$ and on the other hand, the HP filters G2(z) and G3(z) present a band pass in this subband. The filter $G_2(z)$ allows frequencies for $\omega \in \left(\frac{\pi}{4}\,,\ \frac{\pi}{2}\right)$ and the filter $G_3(z)$ allows frequencies for $\omega \in \left(\frac{\pi}{2}\,,\ \frac{3\pi}{4}\right)$. The impulse response of 4CH bank of single filters for DMWT with BiHermite multiwavelet are given by the next equations (61-64) and the transfer functions are shown inn Fig. 12(c).

For the transfer function in Fig. 12(c) it is possible to conclude that the filters $G_0(z)$ and $G_1(z)$ are band stop for$\omega \in \left(\frac{\pi}{4}\,,\ \frac{3\pi}{4}\right)$. The filter with the transfer $\omega \in \left(\frac{\pi}{4}\,,\ \frac{3\pi}{4}\right)$2(z) allows frequencies for $\omega \in \left(\frac{\pi}{8}\,,\ \frac{\pi}{2}\right)$ and the filter $G_3(z)$ appears as an attenuation in the whole frequency band. The value of this attenuation is lowest for $\omega \in \left(\frac{\pi}{2}\,,\ \frac{3\pi}{4}\right)$. The impulse responses for 4CH bank of single filters for DMWT with SA4 multiwavelet are defined by equations (65-68) and their transfer function are shown in Fig. 12(d).

The same as for CL and BiHermite we can conclude that the SA4 multiwavelet filters G0(z) a G1(z) implement approximation subband of DMWT and they are of band pass character for $\omega \in \left(\frac{\pi}{2},\ \frac{3\pi}{4}\right)$. On the other hand, this particular frequency interval is allowed by the filters $G_2(z)$ and $G_3(z)$ which implement detail subband of DMWT. Contrary to the other multiwavelets SA4 multiwavelet shows a significant symmetry of the transfer function.

5.1 Experimental equivalency evaluation of 2CH and 4CH banks for considered multiwavelets

The experiment was performed with 72 images for confirmation of 2CH multifilter and 4CH single filter bank equivalency. These images were transformed by both approaches for all 4 considered multiwavelets. In Tab. 4 mean values of SNR and standard deviation in dB are listed. The value of SNR is computed by (69). Where $I_{\mathrm{MDWT\_2k}}$ represents an image transformed by 2CH bank and $I_{\mathrm{MDWT\_4k}}$ represents an image transformed by 4CH bank.

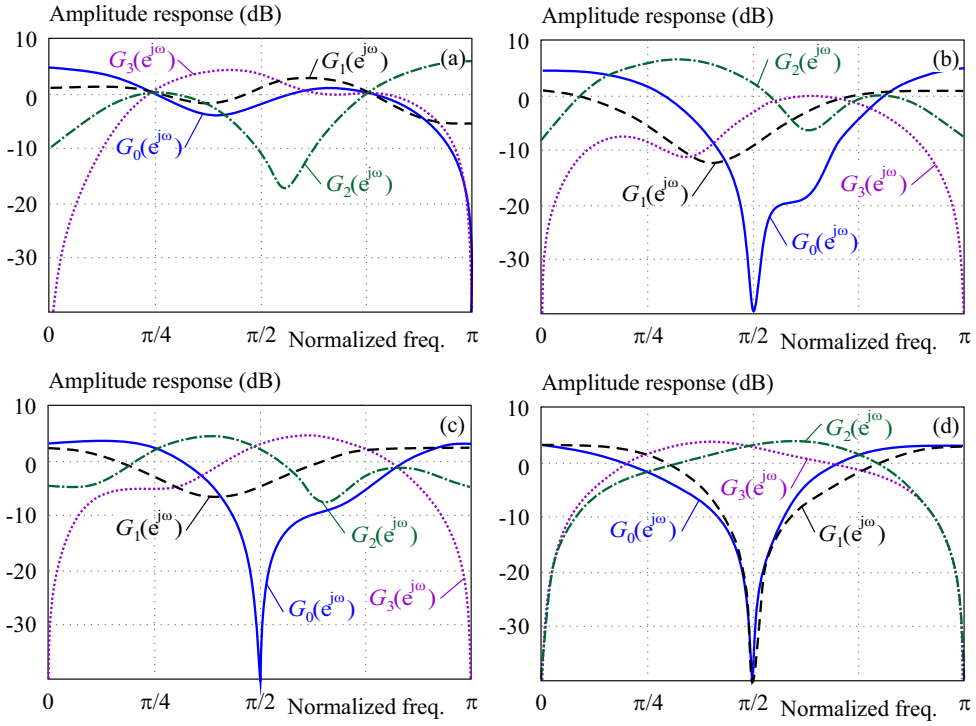

Fig. 12. Transfer functions of 4CH bank of single filters for implementation of DMWT with: (a) – DGHM, (b) — CL, (c) – BiHermite a (d) – SA4 multiwavelet

$$SNR = 10\log\left(\frac{\sum_M \sum_N I^2_{MDWT\_2k}}{\sum_M \sum_N \left(I_{DMWT\_2k} - I_{DMWT\_4k}\right)^2}\right) \tag{69}$$

Table 4. Statistical evaluation of SNR between DMWT implemented by 2CH multifilter bank and 4CH single filter bank

Multiwavelet	Mean value of SNR (dB)	Standard deviation (dB)
DGHM	316.0696	0.3129
CL	318.3322	1.5975
SA4	315.7196	0.8287
BiHermite	317.2854	0.8531

On the base of Tab. 4 it is possible to conclude that the implementations of DMWT performed by 2CH multifilter bank and 4CH single filter bank are equivalent.

6 Possible reduction and combinations of subbands

From the previous chapters it is clear that DWMT produces 4 times more subimages than classical DWT. For purposes of the further processing it is possible to modify this subimage representation in to its reduced form.

The three described modifications of the subimage combinations will be called option 1, 2 and 3.

6.1 All subband reduction (option 1)

This approach reduces all DMWT subbands. From Fig. 13 it can be seen that the approximation coefficients of 4CH DMWT are combined into one channel with the output sequence u(n). The detail coefficients are combined into the sequence v(n) in the same way. By a separate application of this connection on the rows and columns of the image the reduced transformed image is obtained. This transformed image compared to the regular DMWT image has 4 times less subimages as it is possible to observe from Fig. 13(b).

This subimage reduction is useful when it is necessary to compare DMWT with the classical DWT. For example, this option is advantageous for the compression properties comparison. The result of DMWT shown in Fig. 13(b) is very similar to the output of the classical DWT but it needs to be mentioned that the transformed image in Fig. 13(b) is still result of DMWT only with combined subimages. Because the number and arrangement of subimages are comparable to DWT, this option can be used for modification of standard JPEG2000 where the classical DWT with the scalar wavelet (9/7) is used. There is no need for a deep modification of the standard. For modification of JPEG2000 it is sufficient to replace DWT with MDWT with the subband reduction according to option 1. The other blocks of JPEG2000 stay unchanged after this modification. During decoding by the receiver the subbands are easily expanded into the original DMWT shape. The compression properties of DMWT with all the considered multiwavelets and the

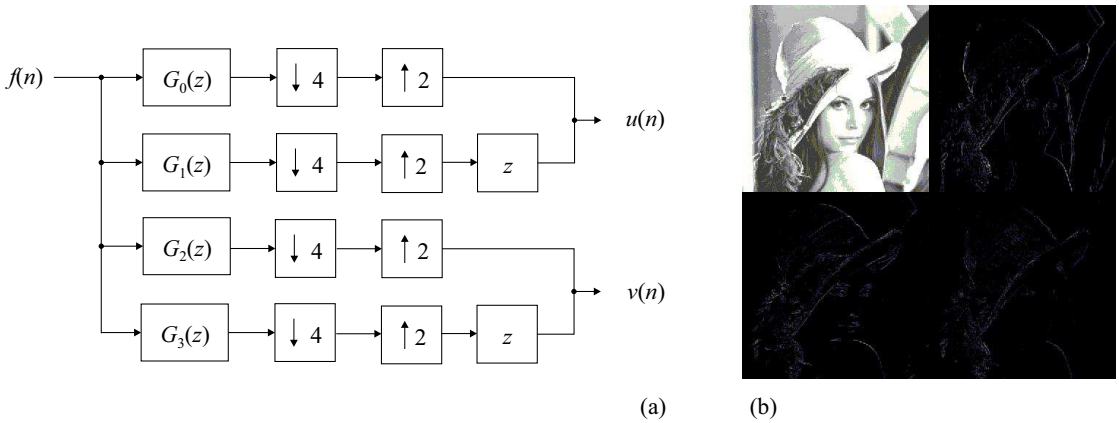

Fig. 13. (a) – block diagram of 4CH equivalent single filter bank with all subband reduction, and (b)– image transformed by DMWT with this reduction

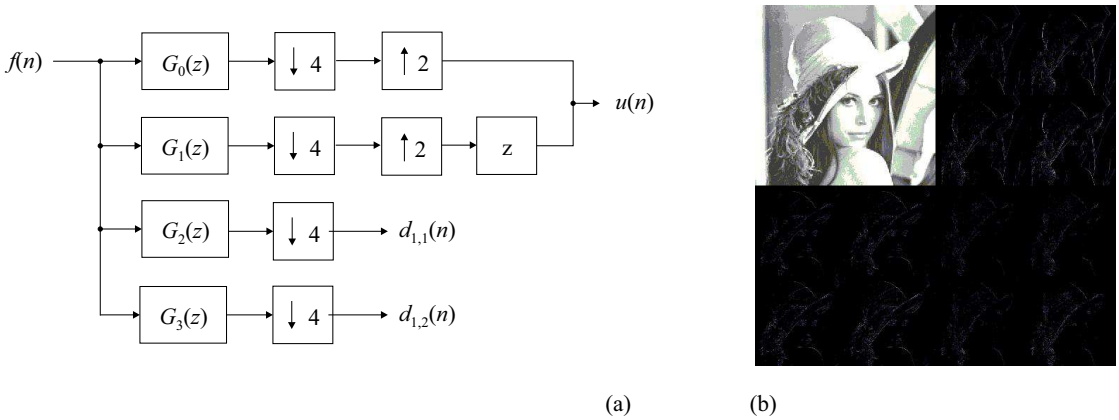

Fig. 14. (a) – block diagram of 4CH equivalent bank with approximation subband reduction, and (b)– DMWT of image with reduction of approximation subbands

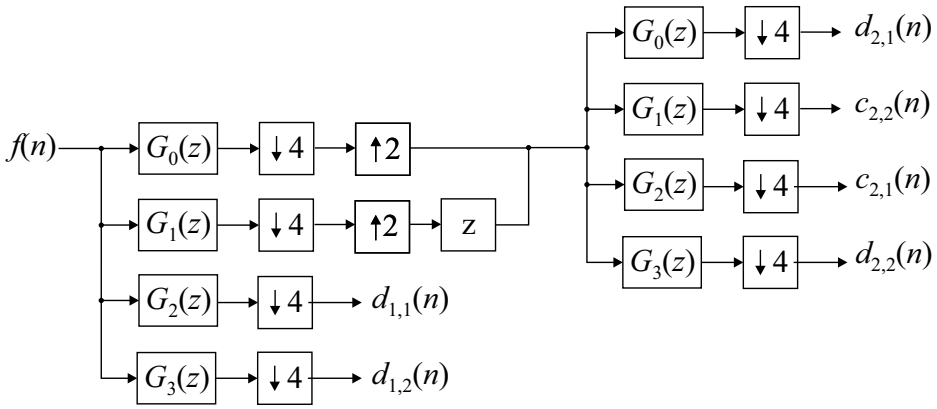

Fig. 15. Block diagram of two level DMWT implemented by 4CH equivalent single filters bank

classical DWT (9/7) are experimentally evaluated in Tab. 5, where mean values and theirs standard deviations of the subband energy distribution are listed. Experiment was performed with 72 input images. The best results were obtained by DMWT with SA4 multiwavelet, where the energy compression into LL subband is the highest, as it can be seen from Tab. 5. Classical DWT with the scalar wavelet (9/7) achieved worse results.

6.2 Approximation subband reduction (option 2)

This modification reduces only number of approximation subbands. The reduction is performed in the same way as in the option 1 but number of detail subbands stays unchanged. The resulting subband combination for DMWT of Lena is shown in Fig. 14(b).

This option can be used for implementation of the second level image transform. DMWT performed by 4CH

single filter bank is applied on the input signal only in one channel in contrast with 2CH multifilter implementation were the second stage is connected directly on two LP outputs (Fig. 3). For 4CH implementation these LP outputs have to be joined as Fig. 15(a) shows. The block diagram of two level DMWT implemented by 4CH single filter bank is shown in Fig. 15. The Lena image transformed by DMWT with 4CH single filter bank is shown in Fig. 16.

Table 5. Statistical evaluation of DMWT and classical DWT energy compression properties

Transform	Subbands	Mean(%)	Std(%)
DGHM	LL	92.277	3.4387
	LH	3.6001	1.3771
	HL	3.6675	1.5912
	HH	0.4559	0.7421
CL	LL	81.905	2.9194
	LH	8.4310	1.0440
	HL	8.4727	1.2217
	HH	1.1920	0.9159
BiHermite	LL	88.095	4.7957
	LH	5.3734	1.7404
	HL	5.5066	2.2439
	HH	1.0251	1.3475
SA4	LL	97.298	4.0311
	LH	1.0849	1.5497
	HL	1.1515	1.8500
	HH	0.4656	0.9883
Wavelet transform (9.7)	LL	97.201	2.1722
	LH	1.4052	1.0400
	HL	1.2384	0.9422
	HH	0.1559	0.4309

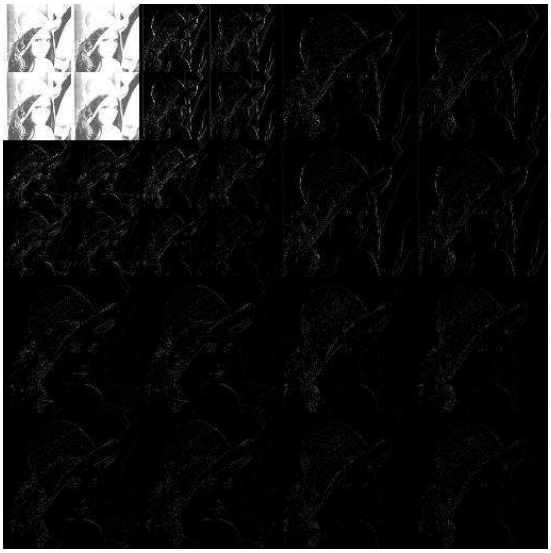

Fig. 16. Two level DMWT of Lena image implemented by 4CH single filters bank

6.3 Detail subband reduction (option 3)

For application of DMWT focused on analysis of approximation subband it is possible to leave the approximation subband unchanged but detail subbands can be reduced. The block diagram of this reduction is shown in Fig. 17(a) and DMWT of the Lena image with detail subimages reduced in this way is shown in Fig. 17(b).

Besides the previously mentioned modifications it is possible perform a reduction only of selected detail subbands. DMWT can be used not only for compression but for other applications as well. One of these applications is classification of textures and objects. In these cases it is often necessary to analyze detail coefficients of the horizontal and vertical detail subimages. The diagonal subimages contain a noise at higher level than the mentioned detail subimages. In this case the subbands $L_1H_1, L_1H_2, L_2H_1, L_2H_2, H_1L_1, H_1L_2, H_2L_1$ and H_2L_2 are analyzed and the subbands H_1H_1, H_1H_2, H_2H_1 and H_2H_2 are reduced into one HH subband. The result of this reduction is shown in Fig. 18.

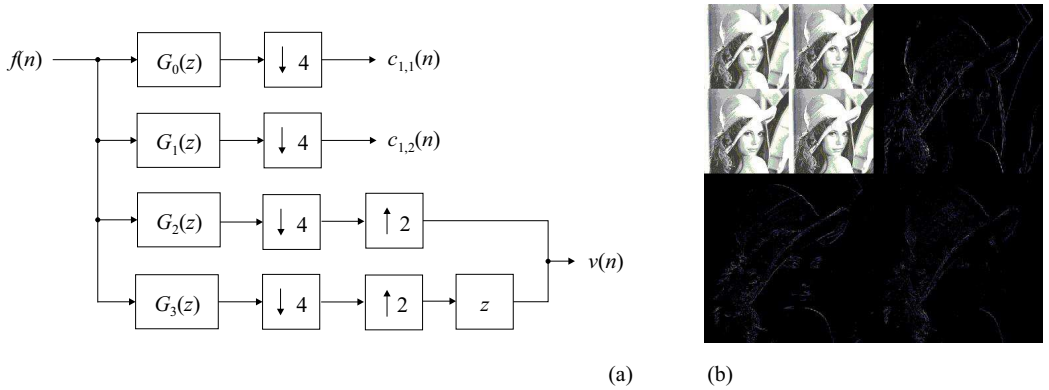

Fig. 17. (a) – block diagram of equivalent filter bank with detail subband reduction and, (b) DMWT of image with this reduction

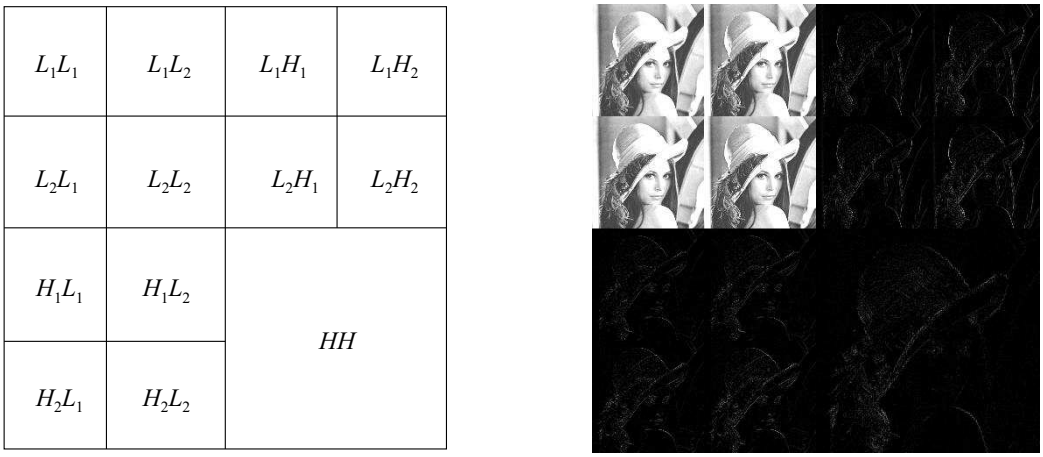

Fig. 18. (a) – combination with reduced HH subband, and (b) – DMWT of image with this reduction

7 Conclusion

The implementations of image DMWT were analyzed in this article. DMWT with multiplicity $r = 2$ implemented by multifilters bank, where impulse responses are defined as matrices of the size 2×2, was discussed in introduction of the article. The implementation of these multifilters by the cross-connected scalar filters was shown in the next part of the article.

By this connection it is possible to perform DMWT for arbitrary multiwavelet functions. The main drawback of this implementation is the need of an input signal prefiltering which splits this signal into 2 inputs of multifilter. The fact that for implementation of DMWT the LP and HP band 8 scalar filters are needed is another drawback. Transfer functions were analyzed in detail for all these scalar filters. The normality of DMWT outputs for the considered multiwavelets was verified on the base of experimental results. For the multiwavelets without normalized outputs the normalization constants were specified and impulse responses of the multifilters were corrected. The compression properties of several multiwavelets were evaluated. From the results it can by concluded that the best energy compression into LP subbands is achieved by DMWT with the SA4 multiwavelet. In the next part of this article the equivalent single filter bank implementation of DMWT was analyzed. The detail mathematical procedure of creation of the single filter impulse responses from the cross-connected scalar filter was described. These single filter bank impulse responses were derived for all the considered multiwavelets. Experimentally was confirmed that the proposed 4CH single filter bank solves the previously mentioned drawbacks of the cross-connected scalar filter bank implementation of DMWT. The transformed image is obtained directly from input image which in this case is not preprocessed by prefilters. The 4 parallel connected filters provide directly 4 outputs belonging to each subband of DMWT outputs. The equivalency of 4CH single filter bank and 2CH multifilter bank was experimentally confirmed as well. The attention in the final part of the article was focused on possible ways of subband combination. There were shown options which can be useful for different MDWT practical applications. The reduction of all subbands provides the output which structurally matches with the output of the classical DWT. This subband combination allows to replace the classical DWT by DMWT in standard JPEG 2000. The experimental results show that DMWT with SA4 multiwavelet achieves a better energy compression into LP subband than the classical DWT with wavelet (9/7). By the reduction of only LP band it is possible to get input for the second level DWMT implemented by 4CH single filter bank. The other mentioned methods of detail subimages combination can be useful in the field of image analysis, object and textures classification.

Acknowledgements

This paper was supported by grant of Faculty of Electrical Engineering and Informatics, Technical University of Košice no. FEI-2018-53.

References

[1] K. Rajakumar and T. Arivoli, "Implementation of Multiwavelet Transform Coding for Lossless Image Compression", *in Proc*, of International Conference on Information Communication Embedded Systems Chennai, 2013.

[2] B. Kai and X. Xiang-Gen, "Image Compression Using a New Discrete Multiwavelet Transform A New Embedded Vector Quantization, *IEEE Transactions on Circuits Systems for Video Technology*, vol. 10, no. 6, pp. 833-842, 2000.

[3] N. Sriraam and R. Shyamsunder, "3-D Medical Image Compression Using 3-D Wavelet Coders", *Digital Signal Processing*, vol. 21, no. 1, pp. 100-109, 2011.

[4] O. Kováč, P. Lukacs, and I. Gladišová, "Textures classification based on DWT", *Radioelektronika - 28th International Conference*, Prague, 2018.

[5] O. Kováč and I. Gladišová, "Multifocal images fusion", *Acta Electrotechnica et Informatica*, vol. 17, no. 3, pp. 22-26, 2017.

[6] T. S. Anand and P. Saravanan, "Performance evaluation of image fusion using the multi-wavelet curvelet transforms", *in IEEE-International Conference On Advances Engineering Science And Management*, 2012.

[7] S. Bhatnagar and R. C. Jain, "Application of Discrete Multiwavelet Transform in Denoising of Mammographic Images", *Indian Journal of Science Technology*, vol. 29, no. 4, pp. 1613-1641, 2016.

[8] V. Bajaj and R. B. Pachori, "Detection of human emotions using features based on the multiwavelet transform of EEG signals", *Brain-Computer Interfaces*, pp. 215-240, 2015.

[9] D. Levický, M. Broda, and V. Hajduk, "Universal statistical steganalytic method", *Journal of Electrical Engineering*, vol. 68, no. 2, pp. 117-124, 2017.

[10] J. Oravec, J. Turán, and Ľ. Ovseník, "DWT Steganography with Usage of Scrambling", *Carpathian Journal of Electronic Computer Engineering*, vol. 9, no. 1, pp. 26-29, 2016.

[11] T.-C. Hsung, D. Lun, Y.-H. Shum, and K. Ho, "Generalized Discrete Multiwavelet Transform with Embedded Orthogonal Symmetric Prefilter Bank", *IEEE Transactions on Signal Processing*, vol. 55, no. 12, pp. 5619-5629, 2007.

[12] C. Chui and J. Lian, "A Study of Orthonormal Multi-Wavelets", *Applied Numerical Mathematics*, vol. 20, no. 3, pp. 273-298, 1996.

[13] V. Kolev, T. Cooklev, and F. Keinert, "Matrix spectral factorization for SA4 multiwavelet", *Multidimensional Systems Signal Processing*, vol. 29, no. 4, pp. 1613-1641, 2018.

[14] O. Kováč, J. Mihalík, and I. Gladišová, "Convolution implementation with a novel approach of DGHM multiwavelet image transform", *Journal of Electrical Engineering*, vol. 68, no. 6, pp. 455-462, 2017.

[15] X.-G. Xia, J. S. Geronimo, D. P. Hardin, and B. W. Suter, "Design of prefilters for discrete multiwavelet transforms", *IEEE Transactions on signal processing*, vol. 44, no. 1, pp. 25-35, 1996.

[16] M. B. Martin and A. E. Bell, "New image compression techniques using multiwavelets multiwavelet packets", *EEE Transactions on image processing*, vol. 10, no. 4, pp. 500-510, 2001.

[17] G. Donovan, J. Geronimo, D. Hardin, and P. Massopust, "Construction of Orthogonal Wavelets Using Fractal Interpolation Functions", *SIAM Journal on Mathematical Analysis*, vol. 27, no. 4, pp. 1158-1192, 1996.

[18] L. Shen, H. H. Tan, and A. J. Y. Tham, "Symmetric-antisymmetric Orthonormal Multiwavelets Related Scalar Wavelets", *Applied Computational Harmonic Analysis*, vol. 8, no. 3, pp. 258 -279, 2000.

[19] H. Guoping and M. Lingjuan, "Cycle-slip detection of GPS carrier phase with methodology of SA4 multi-wavelet transform", *Chinese Journal of Aeronautics*, vol. 25, no. 2, pp. 227-235, 2012.

[20] V. Strela and A. T. Walden, "Orthogonal biorthogonal multiwavelets for signal denoising image compression", *Wavelet Applications V*, vol. 3391, pp. 96-108, 1998.

[21] S. Radhakrishnan and J. Subramaniam, "Novel Image Compression Using Multiwavelets with SPECK Algorithm", *The International Arab Journal of Information Technology*, vol. 5, no. 1, 2008.

[22] The USC-SIPI Image Database,University of Southern California [Online] http://sipi.usc.edu/database [Cit, 27 02 2019].

[23] J. Lebrun and I. Selesnick, "Gröbner bases wavelet design", *Journal of Symbolic Computation*, vol. 37, no. 2, pp. 227-259, 2004.

[24] J. Zavacký and J. Mihalík, "An Algorithm for Calculation of Wavelets by using Quadrature Mirror Filters Bank", *Acta Elektronica at Informatika*, vol. 5, no. 1, pp. 42-50, 2005.

Received 11 March 2019

Ondrej Kováč obtained the MSc in Multimedia telecommunications at the Faculty of Electrical Engineering, Technical University of Košice, in 2011. His PhD thesis topic was focused to texture generating, 3D modeling and coding of human head. Since June 2015, he has been working as assistant professor at the Department of Technologies in Electronics, Technical University of Košice.

Ján Mihalík graduated from the Technical University of Bratislava in 1976. In 1979, he joined the Faculty of Electrical Engineering and Informatics of Technical University of Košice, where he received his PhD degree of radioelectronics in 1985. Currently, he is a full professor of electronics and telecommunications and the head of Laboratory of Digital Image Processing and Videocommunications at Department of Electronics and Multimedia Telecommunications. His research interests include information theory, image and video coding, digital image and video processing and multimedia videocommunications.